JOURNAL OF APPLIED CRYSTALLOGRAPHY
ISSN 1600-5767

Detection of medium-range-order structure in amorphous germanium films by spectroscopic ellipsometry

Xiao-Dong Wang,* Bo Chen, Hai-Feng Wang, Bin Chen, Shi-Jie Liu, Zhong-Xu Cui, Bo Li, Jun-Bo Wang, Shan-Meng Wang and Yun-Peng Li

Changchun Institute of Optics, Fine Mechanics and Physics, Chinese Academy of Sciences, Changchun, 130033, People's Republic of China. *Correspondence e-mail: wangxiaodong@ciomp.ac.cn

Received 8 October 2014
Accepted 19 May 2015

Edited by G. Renaud, CEA-Grenoble DSM/INAC/SP2M/NRS, Grenoble, France

Keywords: amorphous germanium; medium-range order; continuous random networks; spectroscopic ellipsometry.

Amorphous germanium (a-Ge) films in the thickness range of 5.2–370.7 nm were prepared by radio frequency magnetron sputtering. Spectroscopic ellipsometry analysis shows that less than 3% of medium-range order exists in a-Ge under the reported deposition conditions.

1. Introduction

In order to meet the challenge of the serious global energy crisis, many scientists are focusing on solar cells with high conversion efficiency. As key materials in solar cells, tetrahedral amorphous semiconductors [amorphous germanium (a-Ge), amorphous silicon (a-Si)] have attracted renewed interest among researchers owing to their low manufacturing cost and higher efficiencies (Belfedal *et al.*, 2012).

The unique optical and electrical properties of a-Ge have been extensively studied (Blanco *et al.*, 1986; McMarr *et al.*, 1986; Pilione *et al.*, 1987; Goh *et al.*, 2010). It was generally believed that only short-range-order structure exists in tetrahedral amorphous semiconductors. However, Gibson and Treacy found that a-Si and a-Ge contain medium-range order (MRO) by variable coherence microscopy (Gibson & Treacy, 1997; Treacy *et al.*, 1998, 2000). In 2012, Gibson and Treacy conclusively published their revolutionary observations in *Science* that MRO indeed exists in a-Si, and the volume fraction of MRO is approximately 50% (Treacy & Borisenko, 2012*a*; Gibson, 2012). Subsequently, Roorda questioned Treacy's results and argued that the paracrystalline model disagrees with high-resolution X-ray data, while the agreement with fluctuation electron microscopy is at best qualitative (Roorda & Lewis, 2012; Treacy & Borisenko, 2012*b*). After that, based on observations of MRO in a-Ge and a-Si, a Mott–Davis paracrystal model combined with the one-dimensional quantum confinement effect was proposed (Gibson, 2012) to interpret the thickness effect of the bandgap for a-Ge films. We believe that a-Ge has a semiconductor-alloy-like structure, it may contain MRO and continuous random networks (CRNs) simultaneously, and there is a dependence of the MRO/CRN ratio on film thickness and preparation methods/parameters (Wang *et al.*, 2013).

The volume fraction of MRO in tetrahedral amorphous semiconductors is still in controversy (Treacy & Borisenko, 2012*a*; Gibson, 2012; Wang *et al.*, 2013). Thus, it is of practical importance to detect the volume fraction of MRO in tetrahedral amorphous semiconductors. In this paper, 5.2–370.7 nm

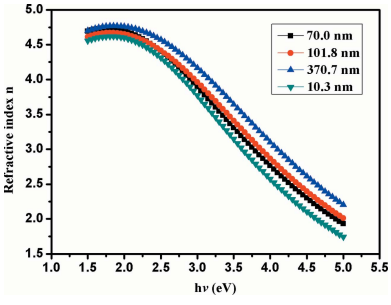

Table 1
SE analysis results of a-Ge films with MRO based on the four-phase models.

d stands for the Ge film thickness characterized by the optical profiling system, d_1 stands for the roughness layer thickness and d_2 stands for the Ge layer thickness.

d (nm)	d_1 (nm)	d_2 (nm)	a-Ge (%)	c-Ge (%)	E_g (eV)	$\varepsilon_1(\infty)$	A (eV)	E_0 (eV)	C (eV)	χ^2
5.2	4.26 (18)	0.01 (3)	98.91 (652)	0.73 (15)	0.821 (39)	0.66 (13)	118 (7)	3.27 (4)	4.13 (9)	0.308
10.3	9.63 (21)	0.64 (4)	90.79 (237)	0.79 (15)	0.809 (17)	0.77 (7)	132 (11)	3.20 (1)	3.95 (5)	0.093
15.4	14.82 (49)	1.29 (7)	97.70 (271)	2.89 (14)	0.827 (9)	1.17 (2)	122 (5)	3.06 (4)	3.64 (7)	0.036
20.6	20.35 (26)	1.47 (5)	94.63 (216)	0.68 (6)	0.889 (7)	1.078 (24)	143 (5)	2.94 (3)	3.59 (2)	0.023
25.7	26.12 (16)	2.60 (7)	95.72 (263)	0.92 (6)	0.919 (8)	1.07 (3)	147 (5)	3.09 (3)	3.98 (3)	0.023
30.8	30.58 (7)	3.92 (10)	95.06 (309)	2.70 (16)	0.963 (8)	1.05 (5)	169 (8)	3.00 (3)	4.13 (3)	0.036
41.1	40.90 (5)	3.78 (5)	92.43 (192)	0.84 (6)	0.864 (10)	1.05 (3)	158 (5)	3.19 (1)	4.14 (2)	0.021
70.0	70.15 (14)	1.63 (11)	98.40 (518)	1.60 (18)	0.801 (19)	1.05 (5)	133 (10)	3.20 (3)	4.18 (3)	0.093
101.8	102.66 (22)	2.43 (11)	95.98 (361)	0.93 (10)	0.826 (7)	0.97 (4)	143 (8)	3.29 (2)	4.25 (3)	0.055
370.7	371.70 (271)	4.75 (30)	94.83 (515)	1.09 (17)	0.808 (17)	0.75 (9)	159 (13)	3.43 (4)	4.44 (6)	0.123

a-Ge films were prepared by radio frequency magnetron sputtering (RF-MS), and the volume of MRO in a-Ge films was detected by spectroscopic ellipsometry (SE). We want to choose a different route to observe the MRO in a-Ge films from the spectral point of view and shed some light on the controversy about MRO in a-Ge.

2. Experiment and method

a-Ge films were fabricated by an RF-MS deposition system (ATC 2200-H, AJA Company, USA) in Ar (99.999%) gas. An RF generator (Seren Company, USA) was used to deposit a-Ge. The Ge (99.999%) target was bought from Kurt J. Lesker Company. The base pressure was 5×10^{-5} Pa, and the working pressure was 0.1 Pa. The sputtering power was kept at 200 W. The a-Ge film was deposited on a 30 mm-diameter fused silica substrate at room temperature. The film thickness was controlled only by deposition time. All film samples were aged for one month prior to optical and electrical characterization.

The film thickness was measured with a NEWVIEW 6000 optical profiling system (ZYGO Company, USA). Film structures were analyzed by SE (UVISEL). This measurement was performed at an incident angle of 70°, and the photon energy range was 1.5–5 eV; the thickness of our substrate was 1.5 mm, and we used a piece of paper to block the incoherent backside reflections according to the SE instruction manual. The reflectance and transmission of the thin films were characterized by a Lambda 950 spectrophotometer in the wavelength range of 700–2000 nm with a step of 1 nm, and the incident angle was fixed at 8°.

3. Results and discussion

In the SE analysis, an appropriate optical dispersion model should be used to describe the optical constants of the a-Ge layer in the spectral fitting. The Tauc–Lorentz model (van den Oever *et al.*, 2007; Jellison & Modine, 1996) has been verified to be a better representation of the dielectric function for amorphous semiconductor films than the Forouhi–Bloomer model (Forouhi & Bloomer, 1986, 1988). In this work, the Tauc–Lorentz model is used to parameterize the optical functions of the a-Ge layer.

Jellison & Modine (1996) presented an expression for the imaginary part of the dielectric function for the Tauc–Lorentz model, which is given by

$$\varepsilon_2(E) = \begin{cases} \left[\dfrac{AE_0C(E-E_g)^2}{(E^2-E_0^2)^2 + C^2E^2}\,\dfrac{1}{E}\right], & E > E_g, \\ 0, & E \le E_g. \end{cases} \quad (1)$$

A, C, E_0 and E_g are four fitting parameters and are all in units of energy. The real part of the dielectric function is derived from the expression for $\varepsilon_2(E)$ using Kramers–Kronig integration and is given by

$$\varepsilon_1(E) = \varepsilon_1(\infty) + \frac{2}{\pi} P \int_{E_g}^{\infty} \frac{\xi\varepsilon_2(\xi)}{\xi^2 - E^2}\,\mathrm{d}\xi, \quad (2)$$

where P is the Cauchy principal part of the integral and $\varepsilon_1(\infty)$ is an additional fitting parameter (Jellison & Modine, 1996).

Fig. 1 illustrates the four-phase model (air/surface-roughness layer/Ge layer/fused silica substrate) employed in the SE analysis of the a-Ge films. For brevity, the model defined in Fig. 1(*a*) is referred to as the CRN model, and that in Fig. 1(*b*) is called the MRO model. The effective dielectric function of the roughness layer and Ge layer is modeled by a Bruggeman effective medium approximation (Bruggeman, 1935). It is well known that there is GeO_2 above the Ge layer (Henrich & Fan, 1975; McMarr & Blanco, 1988; Blanco *et al.*, 1986). Thus, the surface-roughness layer is assumed to be composed of GeO_2 and void. Traditionally, the fractions of the two components in

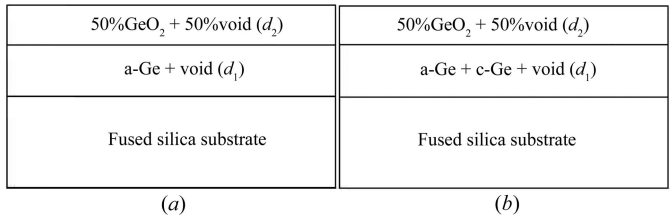

Figure 1
The four-phase models without MRO (*a*) and with MRO (*b*).

Table 2
SE analysis results of a-Ge films without MRO based on the four-phase models.

d stands for the Ge film thickness characterized by the optical profiling system, d_1 stands for the roughness layer thickness and d_2 stands for Ge layer thickness.

d (nm)	d_1 (nm)	d_2 (nm)	a-Ge (%)	E_g (eV)	ε_1 (∞)	A (eV)	E_0 (eV)	C (eV)	χ^2
5.2	4.46 (17)	0.02 (3)	90.29 (480)	0.817 (17)	0.72 (8)	149 (11)	3.22 (1)	4.00 (5)	0.107
10.3	9.70 (40)	0.95 (5)	91.48 (361)	0.830 (10)	1.07 (4)	131 (8)	3.10 (1)	3.70 (2)	0.065
15.4	14.68 (70)	1.19 (10)	99.84 (423)	0.838 (12)	1.09 (3)	126 (8)	3.04 (6)	3.60 (8)	0.067
20.6	21.17 (28)	0.62 (2)	91.28 (220)	0.876 (7)	1.09 (3)	143 (5)	2.95 (3)	3.44 (1)	0.023
25.7	26.58 (14)	2.28 (7)	97.84 (238)	0.915 (7)	1.12 (3)	140 (5)	3.10 (2)	3.86 (3)	0.023
30.8	31.36 (7)	4.25 (7)	98.87 (181)	0.918 (7)	1.16 (3)	146 (4)	3.12 (2)	4.00 (2)	0.018
41.1	40.85 (5)	3.87 (5)	92.41 (220)	0.855 (10)	1.04 (3)	159 (5)	3.22 (1)	4.14 (2)	0.023
70.0	70.28 (16)	1.50 (11)	95.41 (524)	0.816 (20)	0.91 (6)	146 (11)	3.19 (3)	4.17 (3)	0.116
101.8	102.55 (22)	2.60 (12)	96.89 (318)	0.824 (9)	0.96 (5)	143 (7)	3.32 (2)	4.27 (3)	0.059
370.7	370.70 (248)	5.30 (24)	99.20 (559)	0.819 (17)	0.78 (8)	152 (4)	3.49 (3)	4.51 (6)	0.133

the roughness layer are each set to be 50%. The Ge layer is assumed to be a mixture of a-Ge and void for the CRN model, and a-Ge, c-Ge (c in c-Ge stands for crystal) and void for the MRO model (Hazra *et al.*, 2004, 2002). The optical constants of c-Ge are derived from the work of Jellison (1992).

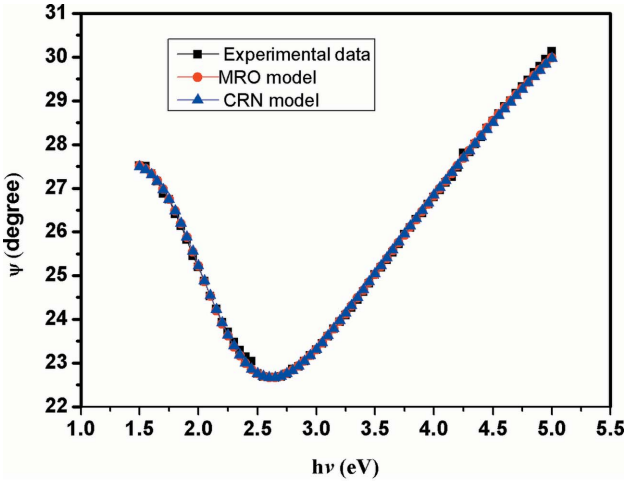

(*a*)

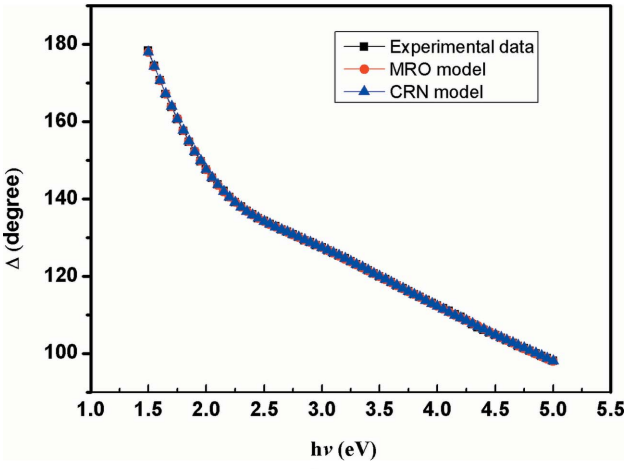

(*b*)

Figure 2
Experimental data and spectral fitting of (*a*) Ψ and (*b*) Δ values for the 41.1 nm a-Ge films. Spectral fittings are based on the four-phase models (MRO model and CRN model).

Table 1 shows the SE analysis results for a-Ge films with MRO based on the four-phase models. Table 2 demonstrates the SE analysis results for a-Ge films without MRO based on the four-phase models. The thickness (d) of the a-Ge films was measured by the optical profiling system, and the error is less than 0.75%. The fractions of void, void%, can be obtained as 100% − (a-Ge%) − (c-Ge%) for the MRO model in Table 1 and 100% − (a-Ge%) for the CRN model in Table 2. We do not give the fraction of void directly in Tables 1 and 2 for simplicity. As shown in Table 1, the volume fraction of c-Ge is 0.68–2.89%, and the MRO model shows no superiority over the CRN model judged by the goodness of fit values represented by χ^2 in the two models. In other words, there is such a low volume fraction of MRO that no significant changes of optical properties are detected by the SE method in the two models.

SE measures the change of the polarization of an incident beam caused by the reflection from the film or substrate surface. The two measured values (Ψ, Δ) are the amplitude ratio and phase difference, respectively, and they are defined by the ratio of amplitude reflection coefficients between p- and s-polarization:

$$\rho = r_p/r_s = \tan\Psi \exp(i\Delta). \quad (3)$$

Fig. 2 demonstrates experimental data and fitting results for Ψ and Δ for the 41.1 nm a-Ge films based on the four-phase models (MRO model and CRN model), and there is a good agreement between experimental data and fitting results. For clarity, only experimental data and fitting results for 41.1 nm a-Ge films are provided. Also, the MRO model shows no superiority over the CRN model. Thus, it is concluded that there is little MRO in our a-Ge films and it is a reasonable assumption that CRN is dominant in our a-Ge samples.

Now we want to verify the correctness of the SE results from three aspects: optical bandgap, film thickness and optical constants.

The optical bandgap of amorphous materials can be obtained by Tauc's equation, which is given by

$$(\alpha h\nu)^{1/n} = B(h\nu - E_g). \quad (4)$$

Here $h\nu$ is the photon energy E, B is the edge width parameter, which is dependent on the structural disorder of the films, α is

Table 3
Bandgaps of 5.2–370.7 nm a-Ge films obtained from Tauc plots and SE analysis.

Thickness d (nm)	$E_{g,opt}$ (eV)	E_g (with MRO) (eV)	E_g (without MRO) (eV)
5.2	0.779	0.821 (39)	0.817 (17)
10.3	0.802	0.809 (17)	0.830 (10)
15.4	0.873	0.827 (9)	0.838 (12)
20.6	0.861	0.889 (7)	0.876 (7)
25.7	0.860	0.919 (8)	0.915 (7)
30.8	0.888	0.963 (8)	0.918 (7)
41.1	0.885	0.864 (10)	0.855 (10)
70.0	0.869	0.801 (19)	0.816 (20)
101.8	0.862	0.826 (7)	0.824 (9)
370.7	0.880	0.808 (17)	0.819 (17)

the absorption coefficient and n is an exponent. For a direct allowed transition, $n = 1/2$; for an indirect allowed transition, $n = 2$; and for a direct forbidden transition, $n = 3/2$. For Ge, known as an indirect semiconductor, n is chosen as 2 (Demichelis *et al.*, 1987; Tsao *et al.*, 2010; Banerjee & Chattopadhyay, 2005). The absorption coefficient can be determined by

$$\alpha = 4\pi k/\lambda, \tag{5}$$

where λ is the wavelength and k is the extinction coefficient, which can be derived from the reflectance and transmittance of the a-Ge films by the *OptiLayer* software (http://www.optilayer.com/), taking into account multiple reflection.

Fig. 3 shows a Tauc plot of $(\alpha E)^{1/2}$ *versus* photon energy E of the a-Ge films. The linear portion is extrapolated to yield the optical bandgap $E_{g,opt}$ at $(\alpha E)^{1/2} = 0$. For the sake of clarity, only the Tauc plots for the 5.2, 15.4 and 41.1 nm a-Ge films were drawn. The values of the bandgap obtained by extrapolating the linear portion of the plots are 0.779, 0.873 and 0.885 eV, respectively. Values of the bandgap for 5.2–370.7 nm a-Ge films derived from Tauc plots and SE analysis are summarized in Table 3. The optical bandgap $E_{g,opt}$ derived from Tauc plots has a 99.9% confidence interval. As shown in

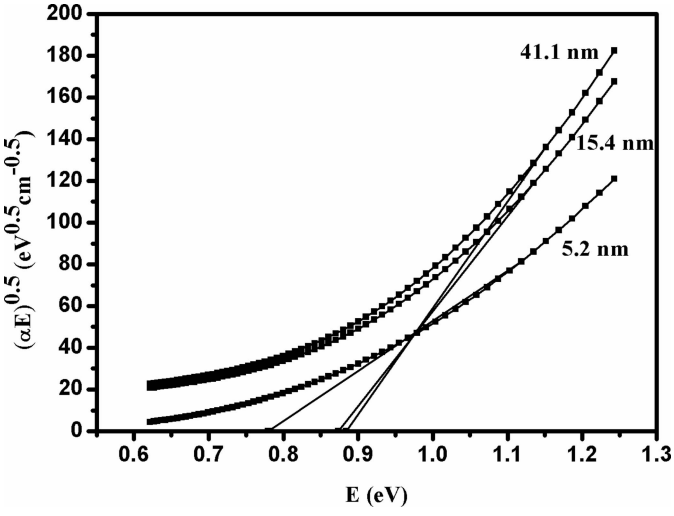

Figure 3
Plot of $(\alpha E)^{1/2}$ *versus* photon energy E for the a-Ge films (5.2, 15.4 and 41.1 nm).

Table 4
Thickness of a-Ge films characterized by the optical profiling system, *OptiLayer* software and SE method.

				SE			
Profiling system		*OptiLayer* software		MRO model		CRN model	
d (nm)	Error	d (nm)	D	d (nm)	χ^2	d (nm)	χ^2
70.0	<0.75%	71.08	0.087	70.15 (14)	0.093	70.28 (16)	0.116
101.8		101.83	0.125	102.66 (22)	0.055	102.55 (22)	0.059
370.7		371.44	0.644	371.70 (271)	0.123	370.70 (248)	0.133

Table 3, the differences in bandgaps from the plots and SE analysis are in the range of 0.007–0.075 eV, which indicates that the SE analysis results are reliable.

The film thicknesses (70.0, 101.8 and 370.7 nm) obtained by the optical profiling system, *OptiLayer* software fitting and SE analysis are summarized in Table 4. D denotes the discrepancy value in the *OptiLayer* software fitting. The difference

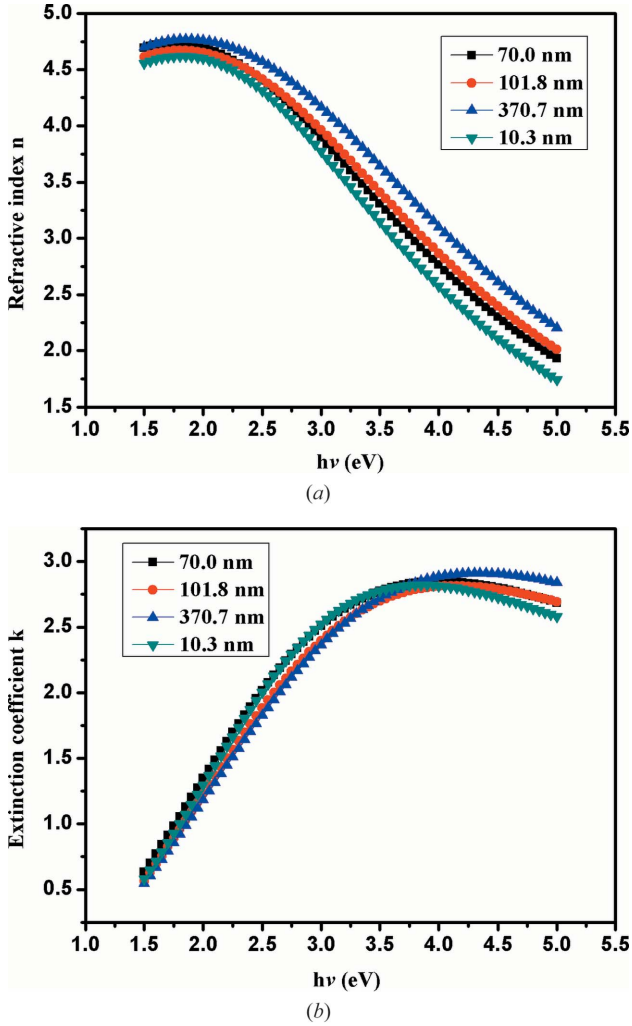

Figure 4
Optical constants of 10.3, 70.0, 101.8 and 370.7 nm a-Ge films: (*a*) refractive index and (*b*) extinction coefficient. The data are derived from an SE analysis based on the CRN model.

between the thickness values is less than 1.4%, which, again, reveals that the results from the SE analysis are reliable.

For clarity, Fig. 4 only shows optical constants of 10.3, 70.0, 101.8, and 370.7 nm a-Ge films. The data are derived from an SE analysis based on the CRN model. The data obtained from the SE analysis based on the MRO model are similar to those based on the CRN model, and thus they are not provided here. The values, shape and trend of optical constants of the a-Ge films characterized by the SE method are very close to those derived from the work of Connell *et al.* (1973) and Donovan *et al.* (1970), which indicates that our SE analysis results are reliable.

Thus, on the basis of our analysis of the bandgap, film thickness and optical constants, it is concluded that there is little MRO in our a-Ge films and it is a reasonable assumption that CRN is dominant in our a-Ge samples.

4. Summary

In summary, MRO and CRN models in SE analysis were used to detect the volume fraction of MRO in a-Ge films with different thicknesses. The SE analysis indicates that less than 3% MRO (as shown in Table 1, the volume fraction of c-Ge is 0.68–2.89%) exists in the a-Ge films deposited by the RF-MS method. The values of bandgap obtained by Tauc plots show a good agreement with those obtained by the SE analysis, and the values of film thickness obtained by the profiling system and *OptiLayer* software fitting demonstrate an excellent consistency with those obtained by SE analysis. These two facts strongly indicate that our SE analysis results are reliable.

Our results are different from the work of Gibson and Treacy, and they believed that the volume fraction of MRO is approximately 50% (Treacy & Borisenko, 2012*a*; Gibson, 2012). The reason for this significant deviation may be that our samples were deposited by RF-MS, while their films were prepared by a thermal evaporation method. Thus, there is a dependence of the volume fraction of MRO on the preparation methods/parameters, and substrate heating may contribute to the formation of MRO structure (Wang *et al.*, 2013).

Acknowledgements

This work is supported by the National Natural Science Foundation of China (grants 10878004, 61077016, 61275152) and the Program of Jilin Provincial Science and Technology Department, China (grant 20116013).

References

Banerjee, A. N. & Chattopadhyay, K. K. (2005). *J. Appl. Phys.* **97**, 1–8.
Belfedal, A., Bouizem, Y., Sib, J. D. & Chahed, L. (2012). *J. Non-Cryst. Solids*, **358**, 1404–1409.
Blanco, J. R., McMarr, P. J., Vedam, K. & Ross, R. C. (1986). *J. Appl. Phys.* **60**, 3724–3731.
Blanco, J. R., McMarr, P. J., Yehoda, J. E., Vedam, K. & Messier, R. (1986). *J. Vac. Sci. Technol. A*, **4**, 577–582.
Bruggeman, D. A. G. (1935). *Ann. Phys.* **416**, 636–664.
Connell, G. A. N., Temkin, R. J. & Paul, W. (1973). *Adv. Phys.* **22**, 659–662.
Demichelis, F., Kaniadakis, G., Tagliaferro, A. & Tresso, E. (1987). *Appl. Opt.* **26**, 1737–1740.
Donovan, T. M., Spicer, W. E., Bennett, J. M. & Ashley, E. J. (1970). *Phys. Rev. B*, **2**, 397–413.
Forouhi, A. R. & Bloomer, I. (1986). *Phys. Rev. B*, **34**, 7018–7026.
Forouhi, A. R. & Bloomer, I. (1988). *Phys. Rev. B*, **38**, 1865–1875.
Gibson, J. M. (2012). *Science*, **335**, 929–930.
Gibson, J. M. & Treacy, M. M. J. (1997). *Phys. Rev. Lett.* **78**, 1074–1077.
Goh, E. S. M., Chen, T. P., Sun, C. Q. & Liu, Y. C. (2010). *J. Appl. Phys.* **107**, 024305.
Hazra, S., Sakata, I., Yamanaka, M. & Suzuki, E. (2002). *Appl. Phys. Lett.* **80**, 4115–4117.
Hazra, S., Sakata, I., Yamanaka, M. & Suzuki, E. (2004). *Phys. Rev. B*, **69**, 235204.
Henrich, V. E. & Fan, J. C. C. (1975). *J. Appl. Phys.* **46**, 1206–1213.
Jellison, G. E. (1992). *Opt. Mater.* **1**(3), 151–160.
Jellison, G. E. & Modine, F. A. (1996). *Appl. Phys. Lett.* **69**, 371–374.
McMarr, P. J. & Blanco, J. R. (1988). *Appl. Opt.* **27**, 4265–4273.
McMarr, P. J., Blanco, J. R., Vedam, K., Messier, R. & Pilione, L. (1986). *Appl. Phys. Lett.* **49**, 328–330.
Oever, P. J. van den, van de Sanden, M. C. M. & Kessels, W. M. M. (2007). *J. Appl. Phys.* **101**, 123529.
Pilione, L. J., Vedam, K., Yehoda, J. E., Messier, R. & McMarr, P. J. (1987). *Phys. Rev. B*, **35**, 9368–9371.
Roorda, S. & Lewis, L. J. (2012). *Science*, **338**, 1539.
Treacy, M. M. J. & Borisenko, K. B. (2012*a*). *Science*, **335**, 950–953.
Treacy, M. M. J. & Borisenko, K. B. (2012*b*). *Science*, **338**, 1539.
Treacy, M. M. J., Gibson, J. M. & Keblinski, P. J. (1998). *J. Non-Cryst. Solids*, **231**, 99–110.
Treacy, M. M. J., Voyles, P. M. & Gibson, J. M. (2000). *J. Non-Cryst. Solids*, **266–269**, 150–155.
Tsao, C. Y., Jürgen, W., Weber, P. C., Conibeer, G., Song, D. & Green, M. A. (2010). *Sol. Energy Mater. Sol. Cells*, **94**, 1501–1505.
Wang, X. D., Wang, H.-F., Chen, B., Li, Y.-P. & Ma, Y.-Y. (2013). *Appl. Phys. Lett.* **102**, 202102.